Dynamic line rating for grid transfer capability optimization in Malaysia

Nurul Husniyah Abas[1], Mohd Zainal Abidin Ab Kadir[1], Norhafiz Azis[1], Jasronita Jasni[1], Nur Fadilah Ab Aziz[2]

[1]Advanced Lightning, Power and Energy Research Centre (ALPER), Faculty of Engineering, Universiti Putra Malaysia, Serdang, Malaysia
[2]Institute of Power Engineering, Universiti Tenaga Nasional, Kajang, Malaysia

Article Info

ABSTRACT

This paper details a case study on the implementation of dynamic line rating (DLR) to enhance the ampacity rating of Malaysia's grid. Utilizing heat balance equations endorsed by the Institute of Electrical and Electronics Engineering (IEEE 738) and the International Council on Large Electric Systems (CIGRE technical brochure 601), the ampacity rating of a Zebra-type aluminum cable steel reinforced (ACSR) conductor on a 275 kV transmission line has been assessed. Real-time weather conditions and conductor temperatures, measured hourly by the DLR sensor over the course of a year, were incorporated into the ampacity calculation to determine the available margin. The weather parameters were analyzed based on the monsoon seasons. A comparative analysis between various methods outlined in the standards and the estimated ampacity rating derived from both standards is presented. According to both standards, the findings indicate that DLR surpasses static line rating (SLR), highlighting the presence of untapped ampacity for grid optimization. Remarkably, CIGRE TB 601 exhibits a higher ampacity rating margin than the IEEE 738 standard, with a percentage difference of 16.20%. The study concludes that the conductor is underutilized and proposes optimization through the integration of real-time weather conditions data into the heat balance equations.

Corresponding Author:

Nurul Husniyah Abas
Advanced Lightning, Power and Energy Research Centre (ALPER), Faculty of Engineering
Universiti Putra Malaysia
Serdang, Selangor, Malaysia
Email: nhusniyahabas@gmail.com

1. INTRODUCTION

The overhead line (OHL) conductor is vital for reliable and uninterrupted electricity transmission from generation sources to end users. To ensure optimal performance, the conductor is subject to a line rating that defines the maximum allowable temperature without compromising safety and causing premature ageing [1]–[3]. The line rating is essential to maintain proper ground clearance and prevent excessive line sagging, which can lead to arcing and faults [3], [4].

Traditionally, line ratings have been determined using a conservative approach known as the static line rating (SLR) [5]. This approach is based on the conductor's heat balance equation and worst-case conditions [6]. The SLR accurately calculates the line rating by considering conservative weather conditions, conductor properties, and load current [1], [3], [4], [7]. The conservative weather conditions, such as low wind speeds (0.446 m/s), full solar radiation (850 W/m^2) and high ambient temperature (35 °C) were

assumed for SLR. However, the reliance on conservative weather conditions leads to underutilizing of the line's current carrying capacity (ampacity) potential [8]. The SLR is becoming less relevant since it fails to consider climate change, integrating renewable energy sources [9], [10], fast-growing demand [11] and conductor ageing, which can increase the risk of forced blackouts. The dynamic line rating (DLR) concept has emerged as a key solution to address these limitations. DLR utilizes real-time weather conditions to determine the line ampacity to optimize the conductor's transfer capability and improve the flexibility of the power system. DLR is also vital in facilitating the energy transition by optimizing grid transfer capacity and integrating renewable energy sources. By accurately assessing the current thermal limits of OHL conductors, DLR empowers grid operators to safely and effectively increase load transfer capacity [12]. This capability is critical in accommodating the intermittent pattern of renewable energy sources like solar and wind power. DLR can also help alleviate congestion issues in the transmission network, where power generation plants are concentrated and far from the main load centres [13], [14].

DLR technology has existed for over two decades, but its recent integration into the grid has become feasible due to technological advancement [3]. Several transmission utilities are implementing DLR, including Oncor electric delivery (United States), Amprion (Germany) [15], Terna (Italy), RTE (France) [16], Elia (Belgium) [3], [17], [18] and Vattenfall (Sweden) [19]. Other countries also have conducted several case studies to demonstrate the performance and reliability of DLR systems. In Canada, it analyzed the DLR system for a wind installation and showed an average 22% capacity increase over SLR 76% of the time [20]. According to case studies in the United Kingdom (UK), DLR integration on all major circuits in England and Wales resulted in a capacity increase of up to 30% [18], [21]. Another study reported that the DLR system in Ireland increased by 0.2 PU rating between 75% and 95% of the time for individual lines [22]. Based on the international experience in Europe, DLR provides capacity increment between 5% to 70% higher than SLR depending on location, due to different weather conditions [21], [23]. It is worth noting that weather conditions in Southeast Asia differ significantly from those in western nations. Therefore, the result of DLR system implementation in Southeast Asia may differ. However, the lack of comprehensive research on DLR implementation in Southeast Asia presents a significant concern, especially given the region's distinct weather patterns during the monsoon season. Only Vietnam [24] and Malaysia [13], [25] have conducted case studies on DLR in Southeast Asia, but these efforts are still in the early stages.

Malaysia is characterized by uniform high ambient temperatures with consistent seasonal variations in wind speed and direction, which are influenced by the monsoon. The monsoon in Malaysia is categorized into four seasons, namely, the southwest monsoon (May-September), the northeast monsoon (November-March), and two shorter periods of inter-monsoon seasons (March-April and October-November). Southwest monsoon (SW) is known as drier weather with minimal monthly rainfall and prevailing wind flow below 7.7 m/s in most Malaysian states. During SW, the wind originates from the southern Indian ocean and the region between Indonesia and Australia. In contrast, the northeast monsoon (NE) season has heavy rainfall with lower ambient temperatures. The wind speed range during the NE season is between 5.2 to 10.3 m/s. The wind comes from Siberia and China's coast towards Malaysia during NE. The inter-monsoon phases in October and April represent transitional periods indicated by light and variable winds. These periods experience the highest average monthly rainfall due to the formation of afternoon thunderstorms aided by clear skies in the morning. The range of solar radiation in Malaysia is between 4.7-6.5 kWh/m^2 [26]–[29].

This paper presents a comprehensive analysis of the heat balance equation proposed by IEEE-738 [30] and CIGRE TB-601 [31], focusing on Malaysia's unique weather conditions. The primary objective is to highlight the available ampacity margin of the 275 kV transmission line by employing the DLR system in the grid. This study investigates the opportunity of using the DLR system in Malaysia during monsoon seasons for grid optimization.

2.   METHOD

The overall framework of this study comprises two main standards to determine the OHL conductor's ampacity rating (I_{max}), as illustrated in Figure 1. The calculated I_{max} values were validated through comparison with the I_{max} value obtained from the DLR sensor. Four parameters need to be acquired to determine the I_{max} at its temperature limit (T_{Cmax}). These parameters were based on the heat balance equation, which consists of convective cooling (q_C and P_c), radiative cooling (q_r and P_r), solar heating (q_s and P_s), and electrical resistance (R_{AC}). I_{max} was determined based on (1) and (2), referencing the IEEE 738 and CIGRE TB 601 standards, respectively.

$$I_{max} = \sqrt{\frac{q_c + q_r - q_s}{R_{AC(T_{Cmax})}}} \tag{1}$$

$$I_{max} = \sqrt{\frac{P_c + P_r - P_s}{R_{AC}(T_{Cmax})}} \qquad (2)$$
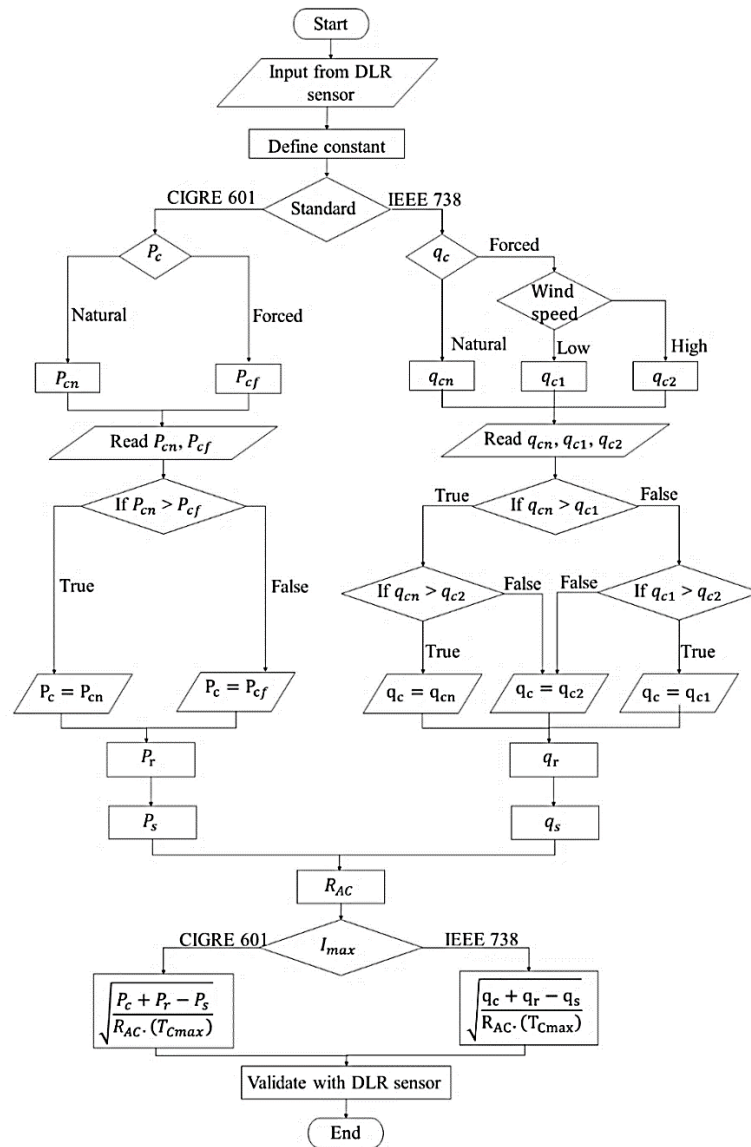
Figure 1. Flowchart for the conductor's I_{max} calculation algorithm

2.1. Convective cooling

q_C and P_c are the main cooling mechanism of the conductor and relies on the participation of wind. q_C and P_c were determined based on (3) to (7), as shown in Table 1. Both IEEE 738 and CIGRE TB 601 standards acknowledge that q_C and P_c can be divided into forced (q_{c1}, q_{c2} and P_{cf}) and natural convective cooling (q_{cn} and P_{cn}).

Table 1. Convective cooling equations as per IEEE 738 and CIGRE 601

Standard	Convective cooling	Wind speed, V_w	Equation	
IEEE 738	Forced	Low, q_{c1}	$K_{angle} \cdot [1.01 + 1.35 \cdot N_{Re}0.52] \cdot k_f \cdot (T_s - T_a)$	(3)
		High, q_{c2}	$K_{angle} \cdot [0.754 \cdot N_{Re}0.6] \cdot k_f \cdot (T_s - T_a)$	(4)
	Natural	Zero, q_{cn}	$3.645 \cdot \rho f^{0.5} \cdot Do^{0.75} \cdot (T_s - T_a)^{1.25}$	(5)
CIGRE TB 601	Forced	High, P_{cf}	$\pi \cdot \lambda_f \cdot (T_s - T_a) \cdot Nu_\delta$	(6)
	Natural	Zero, P_{cn}	$\pi \cdot \lambda_f \cdot (T_s - T_a) \cdot Nu_\beta$	(7)

Based on the IEEE 738 standard, five variables need to be acquired to calculate forced convective cooling at low (q_{c1}) and high wind speeds (q_{c2}) as shown in (3) and (4), respectively. K_{angle} is the wind direction factor, N_{Re} is the Reynolds number, and k_f is the thermal conductivity of air at the average temperature of the boundary layer. The conductor surface temperature (T_s) was set to 75 °C as it is the maximum allowable temperature for Zebra-type aluminum cable steel reinforced (ACSR) conductors. The ambient air temperature (T_a) is based on the real-time measurement from the DLR sensor. The density of air (ρf) was computed for q_{cn} calculation. The outer diameter of the conductor (Do) was set to 0.02862 m [32]. The P_{cf} and P_{cn} were determined based on (6) and (7) for high (P_{cf}) and zero wind speed (P_{cn}), respectively, where λ_f is the thermal conductivity of air at the average temperature of the boundary layer and Nu is the nusselt number.

2.2. Radiative cooling

q_r and P_r are through radiation to the surroundings, ground and sky when the conductor's temperature is higher than the T_a. q_r and P_r were determined based on (8) and (9), as summarized in Table 2. Both standards used the same formula to determine the radiative cooling. q_r and P_r are influenced by four main parameters, which consist of D_O, emissivity (ε), T_S and T_a. The constant 17.8 in IEEE 738 is the product of Stefan-Boltzmann law (σ_B) and Pi (π). The ε value was set to 0.5 in this paper.

Table 2. Radiative cooling equations as per IEEE 738 and CIGRE 601

Standard	Equation	
IEEE 738	$17.8 . D_O . \varepsilon . \left[\left(\dfrac{T_s + 273}{100} \right)^4 - \left(\dfrac{T_a + 273}{100} \right)^4 \right]$	(8)
CIGRE TB 601	$\pi . D_O . \sigma_B . \varepsilon_s . [(T_S + 273)^4 - (T_a + 273)^4 (9)]$	(9)

2.3. Solar heating

q_s and P_s occur when the conductor gains heat energy through exposure to solar radiation. Therefore, the critical variable in solar heating is the value of the conductor's absorptivity (α) which was set to 0.5 as recommended by utilities in Malaysia. q_s by IEEE-738 standard was determined based on (10), where Q_{se} is the total radiated heat intensity corrected for elevation, θ is the effective angle of incidence of the sun's rays and A' is the projected conductor area. In this paper, A' was assumed to be 0.02862 m. In (11) was used to determine the P_s, where I_T is the global solar radiation. q_s and P_s were determined based on (10) and (11), as summarized in Table 3.

Table 3. Solar heating equations as per IEEE 738 and CIGRE 601

Standard	Equation	
IEEE 738	$\alpha . Q_{se} . \sin(\theta) . A' \ (10)$	(10)
CIGRE TB 601	$\alpha . I_T . D \ (11)$	(11)

2.4. Conductor electrical resistance

R_{AC} was determined based on (12). The resistance at high temperature (T_{high}) and low temperature (T_{low}) were set to 8.193^{-5} Ω/m and 6.872^{-5} Ω/m respectively. T_{high}, T_{low} average temperature (T_{avg}) were fixed to 75 °C, 25 °C and 100 °C respectively. Based on (12), the computed $R_{AC}(T_{avg})$ was 8.8535^{-5} Ω/m.

$$R_{AC}(T_{avg}) = \left[\frac{R(T_{high}) - R(T_{low})}{T_{high} - T_{low}} \right] . (T_{avg} - T_{low}) + R(T_{low}) \tag{12}$$

3. CASE STUDY

A Zebra-type ACSR conductor at 275 kV transmission line with a basic span of 365 m was selected in this paper to study the available line ampacity of the conductor. The transmission line was 3 phases, a 50 Hz double circuit with a height of 50 m from the ground. The line direction was 3° to the North. The site for this case study is situated at coordinates 4.350467° latitude and 100.766050° longitude, where the critical line was detected [13]. The configuration and specifications of the conductors used in this case study are shown in Figure 2 and Table 4.
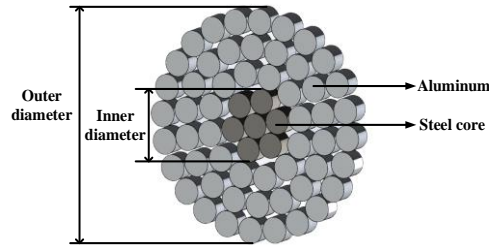
Figure 2. Configuration of Zebra type ACSR conductor

Table 4. Specification of Zebra-type ACSR conductor

Description (symbol)	Value (unit)
DC resistance @20 ℃	0.06740 (Ω)
Outer diameter	0.02862 (m)
Inner diameter	0.00954 (m)
Aluminum wire diameter	0.00318 (m)
Steel core wire diameter	0.00318 (m)
Aluminum wire layers	3

The weather data from the DLR sensor was taken for one year, from January 2021 to January 2022. The line ampacity was analyzed using hourly resolutions. Four weather parameters, namely ambient temperature, solar irradiance, wind speed and wind direction, were considered in this study. The same weather data collected as one-hour average values by the DLR sensor is used in the estimated ampacity calculations performed by MATLAB. An independent comparison was made with DLR calculations performed by the DLR sensor to validate the estimated calculations.

4. RESULT AND DISCUSSION

The additional ampacity of transmission estimate by DLR based on IEEE 738 and CIGRE TB 601 can be seen in Figure 3. The estimated ampacity based on the DLR method is higher than the SLR, indicating a significant margin between both methods. It is expected since the weather-dependent spare capacity is available, and the worst weather conditions assumed by SLR rarely occur [5]. Figure 3 clearly illustrates that the DLR system can increase transmission line ampacity for over 97% of the operational time and remain within the acceptable range. The estimated DLR by both standards surpasses the SLR by less than 2% of the operational time. It implies that the conductor may reach its maximum temperature due to higher loads and escalates the risk of line congestion. The CIGRE TB 601 exhibit a larger margin than IEEE 738. The percentage difference between both standards is 16.20%. These differences are due to distinct ways to calculate solar heat gain and convective cooling. Previous studies indicated that IEEE 738 calculated a lower ampacity rating for conductor sizes less than 1,750 kcmil [33]. The correspondence between the two methods is relatively strong, with acceptable percentage differences. Thus, both approaches are acceptable for the DLR algorithm.
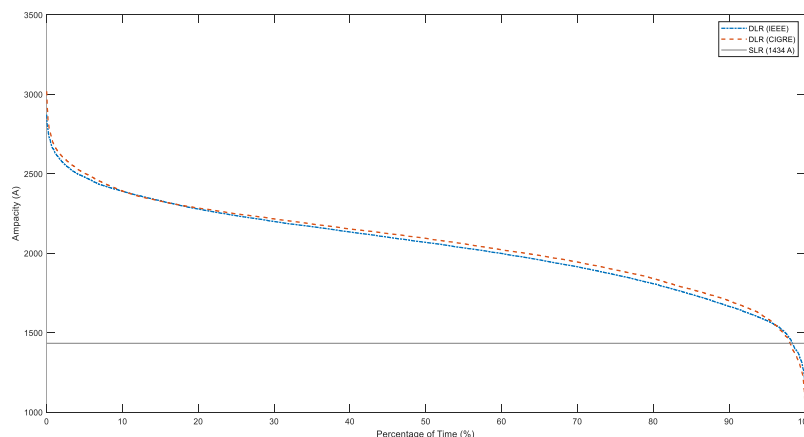

Figure 3. Available ampacity and the SLR OHL for Zebra-type ACSR conductor

The comparison of estimated ampacity rating between MATLAB and DLR sensor can be seen in Figures 4 and 5. The figures show that the load current (purple line) consistently stays below the SLR throughout the performance period. This phenomenon indicates a safe margin between the actual load current and the line's maximum capacity. The percentage differences between the load current with the estimated DLR by IEEE 738 and CIGRE TB 601 are 59.74% and 60.08%, respectively. However, there are specific dates during the year when estimated DLR (orange and blue lines) have approached and exceeded SLR. This situation highlights the importance of monitoring and managing line capacity during these periods to ensure reliable power transmission. The results show that the DLR sensor validates the estimated ampacity rating by DLR by MATLAB as the percentage difference is less than 20% for both approaches. Since the DLR sensor uses the IEEE 738 standard to calculate the DLR, it has a lower percentage difference (6.98%) than CIGRE TB 601 (15.59%).
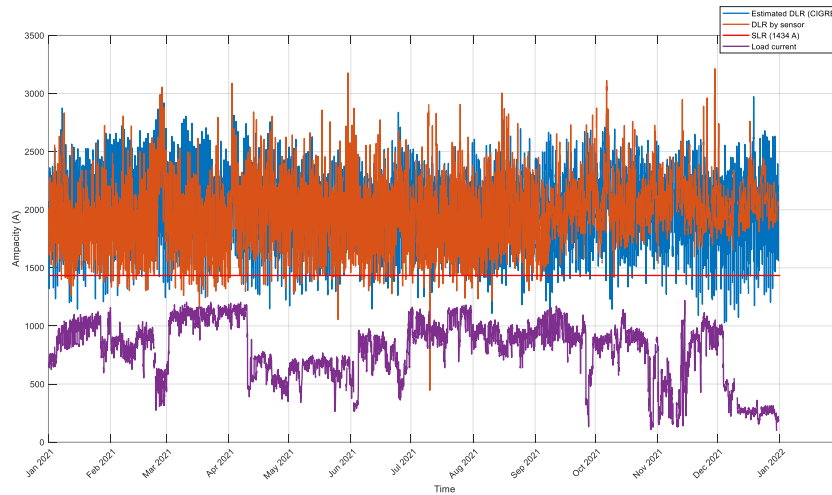
Figure 4. Estimated DLR by IEEE 738 compared to SLR and load current variation throughout the year
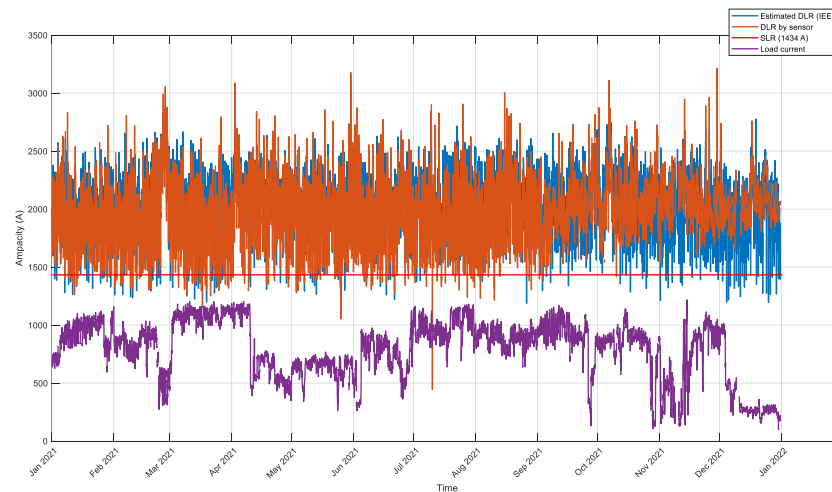
Figure 5. Estimated DLR by CIGRE 601 compared to SLR and load current variation throughout the year

4.1. Wind speed frequency distribution

The wind speed distribution for each monsoon season can be seen in Figure 6. According to the Malaysian Meteorological Department (MET), the wind speed during the SW and NE monsoon is below 7.7 m/s and 10.3 m/s, respectively. During the inter-monsoon seasons, the winds are generally light [27]. The figure presents three ranges of wind speed at the selected transmission line, including low (0.5 m/s), medium (1 to 3 m/s), and medium-high range (3.0 to 4.5 m/s). The medium range has the highest frequency distribution, with more than 40% in all seasons except in the second monsoon. The medium-high wind speed seems insignificant with a frequency distribution less than 5% for all seasons. The range of frequency

distribution for low wind speed is between 8 and 15%, but the value is higher than the assumption made by SLR (0.446 m/s).
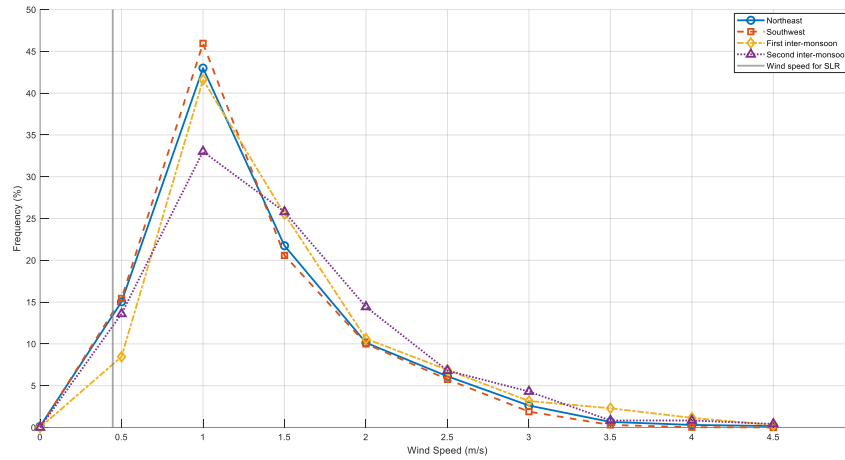

Figure 6. Wind speed distribution

4.2. Wind direction frequency distribution

The wind direction distribution for each monsoon season can be seen in Figure 7. The wind direction is considered with respect to a 90° angle relative to the conductor since the optimal wind direction is 90°. The SW and NE seasons share a similar wind direction pattern, with a 6% frequency distribution between 40° to 60°. During these seasons, wind predominantly attacks the conductor at 80°. In the inter-monsoon seasons, wind direction exhibits a variable pattern, particularly at an angle of more than 50°. This variable pattern is due to the changing direction of the wind direction. The first inter-monsoon has a higher frequency distribution for wind direction less than 40° and declines at wind direction beyond 50°. The second inter-monsoon has the lowest frequency distribution at wind direction between 20° and 60°. The wind direction parallel with the conductor (wind direction=0°) mostly occurs during inter-monsoon seasons.
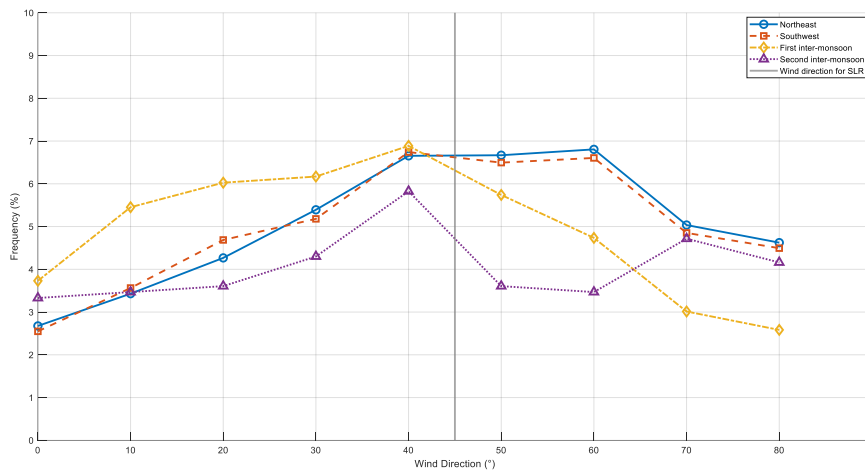
Figure 7. Wind direction distribution

4.3. Solar radiation frequency distribution

The solar radiation distribution for each monsoon season is illustrated in Figure 8. Generally, the frequency distribution of solar radiation follows a pattern where it reaches its highest point at 100 W/m² and then gradually decreases to zero. The conductor experiences the highest solar radiation of 1,000 W/m², which is less than 1%. The lowest solar radiation which is 100 W/m² is between 13% and 15%. The first-inter monsoon has the highest solar radiation, with a main distribution of around 600 W/m² and a 1% frequency

distribution of 1,000 W/m^2. Other seasons have the similar pattern of solar radiation with main distribution between 400 and 500 W/m^2. The line experiences higher solar radiation than assumed solar radiation at SLR, 850 W/m^2, which is less than 2% for all seasons, except the first-inter-monsoon season which is less than 4%.
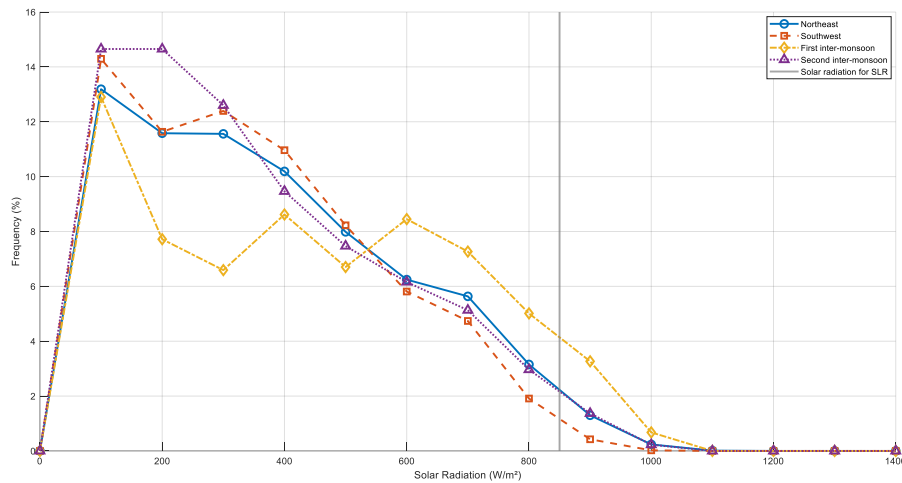

Figure 8. Solar radiation distribution

4.4. Ambient temperature frequency distribution

The ambient temperature distribution for each monsoon season can be seen in Figure 9. Throughout all seasons, the conductor experiences ambient temperatures ranging from 20 °C to 30 °C. The frequency of conductor encounters with 30 °C ambient temperature is less than 20%. The highest frequency distribution is between 50% and 60% for the ambient temperature of 25°. The ambient temperature never reaches 35 °C as assumed by SLR as the worst-case condition. The NE season has the lowest ambient temperatures, with the highest frequency distribution at 20 °C. In contrast, the first inter-monsoon season has the highest frequency distribution in the 25 °C to 30 °C compared to the other seasons. It is worth noting that the ambient temperature is relatively constant throughout the year, with less than a 10% percentage difference between the seasons.
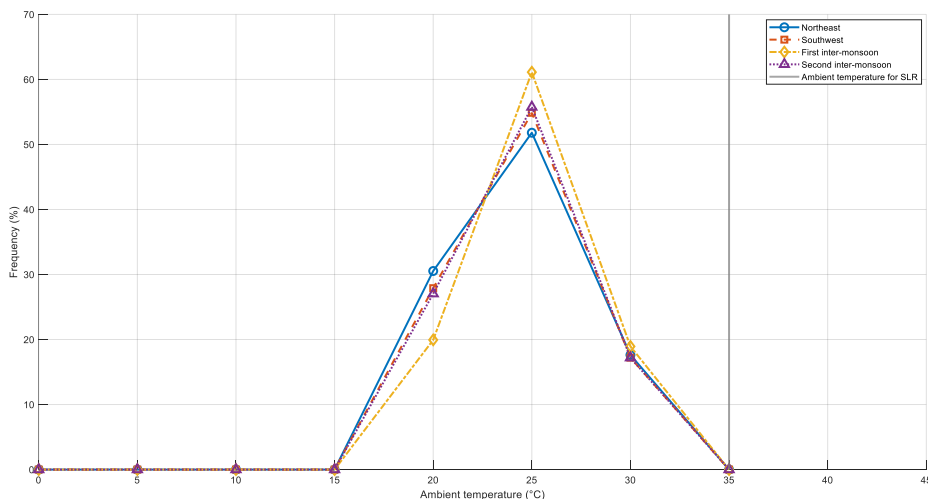
Figure 9. Ambient temperature distribution

4.5. Conductor temperature frequency distribution

The conductor temperature throughout the year to ensure it operates comfortably within safe limits can be seen in Figure 10. The conductor temperature mainly falls within the range of 30 °C to 40 °C and

remains below the maximum allowable temperature for the Zebra-type ACSR conductor, whereby 75 °C. This result implies that the conductor temperature maintains a safe margin of over 40%. The second inter-monsoon season has the highest frequency distribution for conductor temperature at 50 °C and operates at temperatures below 30 °C less frequently than other seasons. In contrast, the first inter-monsoon season exhibits a higher frequency distribution for conductor temperature at 50 °C. The southwest and northeast seasons show a similar pattern with slight differences in frequency distribution. Assessing the influence of weather conditions and conductor temperature is crucial in integrating the DLR system into the grid.
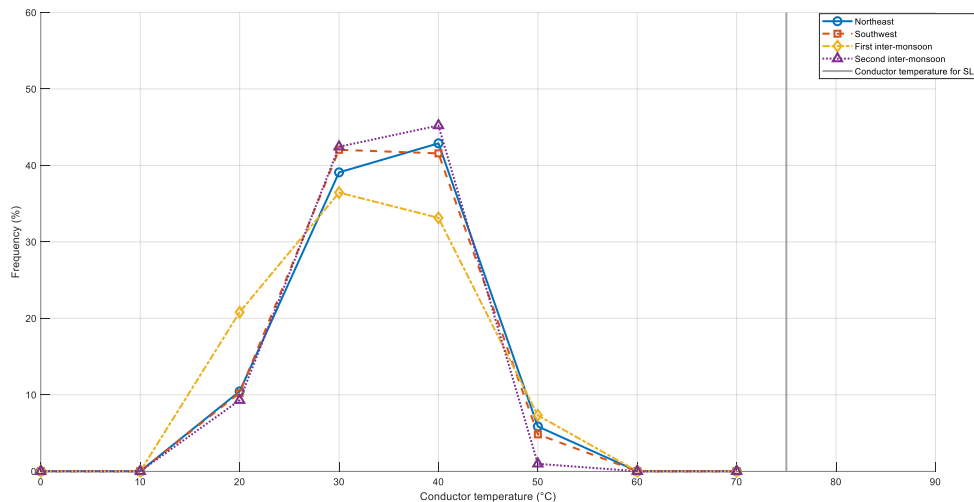
Figure 10. Conductor temperature distribution

5. CONCLUSION

In conclusion, analysis of Malaysia's 275 kV transmission line shows that DLR can optimize the grid capacity. According to estimated ampacity based on IEEE 738 and CIGRE TB 601 standards validated by the DLR sensor, the results demonstrate sufficient available capacity. The ampacity rating in CIGRE TB 601 is 16.20% higher than in IEEE 738. The weather conditions, including wind speed, wind direction, solar radiation and ambient temperature, indicate that the transmission line operates comfortably according to the monsoon seasons. The conductor temperature consistently remains below 60 °C throughout the year, representing that the conductor is underutilized and can be optimized.

REFERENCES

[1] A. Dino, A. Ketley, and G. Mcdougall, "Dynamic transmission line rating technology review, Hydro Tasmania Consulting, Tasmania, Australia," no. July, 2009.
[2] M. Merante, "Application of dynamic rating to improve transportation capability of the power systems connected to wind power plants," no. September, p. 32, 2016.
[3] P. Schell, "Dynamic line rating (DLR)," *Renewable Energy Integration*, no. June, pp. 405–411, 2014, doi: 10.1016/b978-0-12-407910-6.00032-6.
[4] M. Kanálik, A. Margitová, and Ľ. Beňa, "Temperature calculation of overhead power line conductors based on CIGRE Technical Brochure 601 in Slovakia," *Electrical Engineering*, vol. 101, no. 3, pp. 921–933, Sep. 2019, doi: 10.1007/s00202-019-00831-8.
[5] O. Dzobo and H. Tazvinga, "Impact of weather conditions on line ampacity of overhead transmission lines," in *2019 9th International Conference on Power and Energy Systems, ICPES 2019*, Dec. 2019, pp. 1–5, doi: 10.1109/ICPES47639.2019.9105637.
[6] A. Chaichana, "Computation of dynamic line rating of overhead transmission line using weather forecast and interval arithmetic," in *Proceedings - 2018 IEEE International Conference on Environment and Electrical Engineering and 2018 IEEE Industrial and Commercial Power Systems Europe, EEEIC/I and CPS Europe 2018*, Jun. 2018, pp. 1–4, doi: 10.1109/EEEIC.2018.8493657.
[7] L. Staszewski and W. Rebizant, "The differences between IEEE and CIGRE heat balance concepts for line ampacity considerations," *Proceedings - International Symposium: Modern Electric Power Systems, MEPS'10*, 2010.
[8] K. Milad, "Economic dispatch using advanced dynamic thermal rating," University of Alberta, Edmonton, Canada, 2011.
[9] K. Morozovska and P. Hilber, "Study of the monitoring systems for dynamic line rating," *Energy Procedia*, vol. 105, pp. 2557–2562, May 2017, doi: 10.1016/j.egypro.2017.03.735.

[10] S. A. Razzaq and V. Jayasankar, "Energy management system for AC/DC HMGS integrated with interconnected renewable sources and interlinking converter," *International Journal of Applied Power Engineering*, vol. 12, no. 1, pp. 24–36, Mar. 2023, doi: 10.11591/ijape.v12.i1.pp24-36.

[11] H. B. Sassi, Y. Mazzi, F. Errahimi, and N. Es-Sbai, "Power transfer control within the framework of vehicle-to-house technology," *International Journal of Electrical and Computer Engineering*, vol. 13, no. 4, pp. 3817–3828, Aug. 2023, doi: 10.11591/ijece.v13i4.pp3817-3828.

[12] L. Dahlgren, "Case study on applications of measurement equipment for dynamic line rating," KTH Royal Institute of Technology, 2020.

[13] M. H. A. Aziz, N. S. Miswan, F. A. Farah, M. S. M. Shokri, M. N. Noran, and A. A. Rahim, "Pilot project on dynamic line rating (DLR) system for optimal use of tenaga nasional berhad (TNB) grid capacity," in *Proceeding - 2nd International Conference on Technology and Policy in Electric Power and Energy, ICT-PEP 2020*, Sep. 2020, pp. 77–81, doi: 10.1109/ICT-PEP50916.2020.9249936.

[14] J. Cardenas, S. Dominguez, and R. Kommu, "Experiences in dynamic line rating (DLR) using a wireless line monitoring system (ILMS)," in *IET Conference Publications*, 2020, vol. 2020, no. CP771, pp. 6 pp.-6 pp., doi: 10.1049/cp.2020.0140.

[15] P. Glaum and F. Hofmann, "Enhancing the German transmission grid through dynamic line rating," in *International Conference on the European Energy Market, EEM*, Sep. 2022, vol. 2022-September, pp. 1–7, doi: 10.1109/EEM54602.2022.9921148.

[16] E. Cloet, J. L. Lilien, and P. Ferrieres, "Experiences of the Belgian and French TSOs using the 'Ampacimon' real-time dynamic rating system," *43rd International Conference on Large High Voltage Electric Systems 2010, CIGRE 2010*, 2010.

[17] R. Dupin and A. Michiorri, "Dynamic line rating forecasting," in *Renewable Energy Forecasting: From Models to Applications*, Elsevier, 2017, pp. 325–339.

[18] D. Kladar, X. Associates, and U. St, "Dynamic line rating in the world - Overview," XpertPower Associates Ltd., United States, February 2014, 2016.

[19] A. Bergström and E. Torkildsson, "Experiences from dynamic line rating pilot installations in vattenfall distribution´s 145 kV system," in *Sweden, Study Committee B5 Cooloquium, Auckland, New Zealand*, Sept. 2017.

[20] P. Schell, J. Lambin, B. Godard, M. Nguyen, and L. Lilien, "Using dynamic line rating to minimize curtailment of wind power connected to rural power networks," in *Proceedings of the 10th International Workshop on Large-Scale Integration of Wind Power into power systems*, Aarhus, Denmark, 2011.

[21] T. B. Phillips, "Dynamic rating of transmission lines for improved wind energy integration in complex terrain," *Boise State University*, May, 2014.

[22] B. Keyvani, E. Whelan, E. Doddy, and D. Flynn, "Indirect weather-based approaches for increasing power transfer capabilities of electrical transmission networks," *Wiley Interdisciplinary Reviews: Energy and Environment*, vol. 12, no. 3, May 2023, doi: 10.1002/wene.470.

[23] World Bank Group, *Smart Grid to Enhance Power Transmission in Vietnam*. World Bank, Washington, DC, 2016.

[24] X. T. Nguyen and T. D. Nguyen, "Dynamic line rating solution: deployment opportunities for the power transmission grid of Vietnam," *International Journal of Energy and Power Engineering*, vol. 11, no. 2, p. 56, 2022, doi: 10.11648/j.ijepe.20221102.15.

[25] M. S. M. Shokri, F. A. M. Kasran, M. H. A. Aziz, N. S. Miswan, M. N. Noran, and A. A. Rahim, "Dynamic line rating (DLR) by weather-based calculation for power grid optimization in tenaga nasional berhad (TNB)," in *HONET 2020 - IEEE 17th International Conference on Smart Communities: Improving Quality of Life using ICT, IoT and AI*, Dec. 2020, pp. 113–117, doi: 10.1109/HONET50430.2020.9322810.

[26] World Bank Group, "Climate risk country profile: Malaysia," *Asian Development Bank*, pp. 1–28, 2021, [Online]. Available: www.worldbank.org.

[27] Z. Nizamani, K. C. Thang, B. Haider, and M. Shariff, "Wind load effects on high rise buildings in Peninsular Malaysia," *IOP Conference Series: Earth and Environmental Science*, vol. 140, no. 1, p. 012125, Apr. 2018, doi: 10.1088/1755-1315/140/1/012125.

[28] A. K. Amirruddin, M. M. Noor, K. Kadirgama, and K. V. Sharma, "The potential of wind and solar energy in malaysia east coast: Preliminary study at Universiti Malaysia Pahang (UMP)," in *WIT Transactions on Ecology and the Environment*, Dec. 2011, vol. 148, pp. 475–482, doi: 10.2495/RAV110431.

[29] J. O. Petinrin and M. Shaaban, "Renewable energy for continuous energy sustainability in Malaysia," *Renewable and Sustainable Energy Reviews*, vol. 50, pp. 967–981, Oct. 2015, doi: 10.1016/j.rser.2015.04.146.

[30] IEEE "Power Engineering Society," *IEEE standard for calculating the current-temperature relationship of bare overhead conductors*, vol. 2006, no. January, 2012.

[31] Iglesias *et al.,* "Guide for thermal rating calculations of overhead lines," CIGRE, Paris, France, 2014.

[32] Z. Shukri, N. S. Nik Yusuf, D. M. Noor, S. K. S. Abdullah, and M. F. Yahaya, "Guide on Overloading of TNB Overhead Transmission Lines," no. EG310808-OHL_OVERLOAD, Version 1.1, pp. 1–74, 2008.

[33] N. P. Schmidt, "Comparison between IEEE and CIGRE ampacity standards," *IEEE Transactions on Power Delivery*, vol. 14, no. 4, pp. 1555–1559, doi: 10.1109/61.796253.

BIOGRAPHIES OF AUTHORS

Nurul Husniyah Abas 🆔 🇬 🆂🅲 ↻ received her B.Eng. degree in Electrical and Electronic Engineering from Universiti Putra Malaysia. Currently, she is a Ph.D. student in Electrical Power Engineering at the Faculty of Engineering, Universiti Putra Malaysia. She is a Graduate Member of the Board of Engineers Malaysia (BEM). She can be contacted at email: nhusniyahabas@gmail.com.

Mohd Zainal Abidin Ab Kadir received his B.Eng. degree in Electrical and Electronic Engineering from Universiti Putra Malaysia and Ph.D. degree in High Voltage Engineering from the University of Manchester, UK, respectively. Currently, he is a Professor at the Faculty of Engineering, Universiti Putra Malaysia. He is the Founding Director at the Centre for Electromagnetic and Lightning Protection Research (CELP), Universiti Putra Malaysia. He is a Fellow of the Academy of Sciences Malaysia and Fellow of the IET. He is also an IEEE power and energy society (PES) distinguished Lecturer in the Field of Lightning and High Voltage Engineering. To date he has authored and co-authored over 450 journals and conference papers. His research interests include high voltage engineering, lightning protection, electromagnetic compatibility and grid of the future. He can be contacted at email: mzk@upm.edu.my.

Norhafiz Azis received the B.Eng. degree in Electrical and Electronic Engineering from Universiti Putra Malaysia in 2007, and Ph.D. degree in Electrical and Electronic Engineering with a focus on power transformer from The University of Manchester, U.K. Currently, he is an Associate Professor at the Faculty of Engineering, Universiti Putra Malaysia. He is the head of the Advanced Lightning, Power and Energy Research (ALPER). His research interests include in-service aging of transformer insulation, condition monitoring, asset management, and alternative insulation materials for transformers. He can be contacted at email: norhafiz@upm.edu.my.

Jasronita Jasni received the M.Eng. degree in Electrical Engineering from Universiti Teknologi Malaysia in 2001 and Ph.D. degree in Electrical Power Engineering from Universiti Putra Malaysia in 2010. Currently, she is an Associate Professor at the Faculty of Engineering, Universiti Putra Malaysia. Her research interests include power system analysis for static and dynamics, load flow analysis, embedded generation, and renewable energy. She can be contacted at email: jas@upm.edu.my.

Nur Fadilah Ab Aziz received her M.Eng. degree (Hons.) in Electrical Engineering from the University of Southampton, UK in 2006 and her Ph.D. degree from Universiti Teknologi Mara, Shah Alam in 2014. Currently, she is a Senior Lecturer at the Department of Electrical and Electronics Engineering, Universiti Tenaga Nasional (UNITEN), Malaysia. She is also a Graduate Member of the Board of Engineers Malaysia (BEM). Her research interests include power system analysis, renewable energy, fault identification and location, distribution automation, statistical pattern recognition, artificial intelligence (AI) and machine learning applications in the power system. She can be contacted at email: NFadilah@uniten.edu.my.